Dynamics of quantized vortices in Bose-Einstein condensates with laser-induced spin-orbit coupling

Kenichi Kasamatsu
Department of Physics, Kinki University, Higashi-Osaka, 577-8502, Japan
and Institut für Theoretische Physik, Leibniz Universität Hannover, 30167 Hannover, Germany
(Dated: October 2, 2015)

We study vortex dynamics in trapped two-component Bose-Einstein condensates with a laser-induced spin-orbit coupling using the numerical analysis of the Gross-Pitaevskii equation. The spin-orbit coupling leads to three distinct ground state phases, which depend on some experimentally controllable parameters. When a vortex is put in one or both of the two-component condensates, the vortex dynamics exhibits very different behaviors in each phase, which can be observed in experiments. These dynamical behaviors can be understood by clarifying the stable vortex structure realized in each phase.

PACS numbers: 03.75.Lm, 03.75.Mn, 67.85.Fg

arXiv:1510.00142v1 [cond-mat.quant-gas] 1 Oct 2015

I. INTRODUCTION

Experimental realization of spin-orbit (SO) coupled Bose-Einstein condensates (BECs) in cold atoms have opened a new avenue of studying rich dynamical behaviors in new quantum fluids [1–4]. The coupling of the momentum and spin degrees of freedom may yield new structure of topological defects. Quantized vortices in atomic BECs have been thoroughly studied for past decades [5], but those in SO coupled BECs are a quite new topic. It has been shown that a coreless vortex referred to as a half-quantized vortex (HQV) can be the ground state for a small condensate with a symmetric two-dimensional (2D) SO coupling known as the Rashba-type [6–8]. Also, some studies considered the vortex structures in SO coupled BECs in a rotating trap [9–11].

Experimentally, the SO coupling can be synthesized by the laser-induced Raman coupling between different hyperfine states of atoms, which realizes a 1D SO coupling corresponding to the combination of equal weight of the Rashba- and Dresselhaus-type coupling [1, 12–14]; a recent experiment has demonstrated creation of a 2D synthetic SO coupling for cold atoms [15]. The laser-induced SO coupling realized in the experiments provides rich physics of the BECs and much of these properties have been studied [4, 16–22]. Recently, Fetter has considered the dynamics of a single vortex in trapped BECs with the laser-induced SO coupling, giving characteristic features of the dynamics based on the time-dependent Lagrangian formalism [23]. Although there remains an experimental difficulty to create a vortex in the SO coupled condensate by using a rotating trap as done before [9], the vortex creation without rotation may be possible by the rapid thermal quench of the atomic gas into the condensation regime [23, 24]. Real time dynamics of vortices was observed through the snapshots of the condensate density, where successive short microwave pulses were applied to transfer a small fraction of condensed atoms to the untrapped state [25].

In this paper, we study the vortex dynamics in laser-induced SO coupled BECs through the numerical simulations of the 2D Gross-Pitaevskii (GP) equation. There are three distinct phases for the BECs with the Raman-induced SO coupling, namely the stripe phase, the plane-wave phase, and the mixed phase [4, 16, 17]. These phases can be stabilized by changing the Rabi frequency that depends on the strength of the Raman laser beam. We study the vortex dynamics when a single vortex is put in one or both of the components. The vortex structure in each phase is strongly dependent on the energetic constraint caused by both the SO coupling and the Rabi coupling. As a result, vortex dynamics exhibits a quite different behavior in each phase.

This paper is organized as follows. Section II introduces the basic formulation of the SO coupled BECs and addresses briefly the ground state property of this system, which is necessary to understand the following discussion. In Sec. III, we show results of our numerical simulations of the vortex dynamics in the three phases of the SO coupled BEC. Section IV devoted to the discussion and conclusion.

II. BASICS

A. Formulation for Raman-induced SO coupled BECs

We consider a 2D system of two-component (psudospin-1/2) BECs with a laser-induced SO coupling [1] to study the vortex dynamics. The single-particle SO Hamiltonian has the 2×2 matrix structure

$$h_0 = \frac{\hbar^2}{2m}\left(-i\boldsymbol{\nabla}\sigma_0 + k_0\hat{\mathbf{x}}\sigma_z\right)^2 + \frac{\hbar\delta}{2}\sigma_z + \frac{\hbar\Omega}{2}\sigma_x + V_{\rm tr}\sigma_0. \quad (1)$$

Here, m is the atomic mass, σ_r for $r = x, y, z$ is one of the Pauli matrices and σ_0 is the unit matrix. The trapping potential is assumed to be a harmonic form $V_{\rm tr} = m\omega_\perp^2 r^2/2$. As discussed in Ref. [1], this spinor Hamiltonian has three parameters under experimental control: k_0 is the wavenumber of the Raman laser beams,

Ω is the associated Rabi frequency related to the intensity of the laser beams, and δ is the detuning controlled by an external magnetic field. The kinetic energy term has a uniform synthetic gauge field $-\hbar k_0 \hat{\mathbf{x}}\sigma_z$ proportional to the spin matrix σ_z. This term represents the 1D SO coupling along the x-direction whose magnitude can be controlled by k_0.

The Lagrangian and the energy functional including the single-particle SO Hamiltonian of Eq. (1) is given by

$$L = \int d^2r \frac{i\hbar}{2}\left(\Psi^\dagger \frac{\partial \Psi}{\partial t} - \frac{\partial \Psi^\dagger}{\partial t}\Psi\right) - E[\Psi], \tag{2}$$

$$E[\Psi] = \int d^2r \left(\Psi^\dagger h_0 \Psi + \frac{g}{2}\sum_{j=1,2}|\Psi_j|^4 + g_{12}|\Psi_1|^2|\Psi_2|^2\right). \tag{3}$$

The order parameters are represented by the 2-component spinor $\Psi = (\Psi_1, \Psi_2)^T$. Here, we set the same intracomponent coupling constant as g for simplicity, and gives $g_{12}/g \equiv \gamma = 0.995$ according to the parameters of the ^{87}Rb atoms [1]. This small difference between g and g_{12} is important to stabilize the stripe phase in the SO coupled BECs [17]. We scale the energy using the recoil energy $E_R = \hbar^2 k_0^2/2m$ with the wave number k_0 of the Raman photon. Taking the length scale by k_0^{-1}, we have

$$\tilde{h}_0 = (-i\nabla\sigma_0 + \hat{\mathbf{x}}\sigma_z)^2 + \frac{\tilde{\delta}}{2}\sigma_z + \frac{\tilde{\Omega}}{2}\sigma_x + \tilde{V}_{\rm tr}\sigma^0, \tag{4}$$

where the dimensionless quantities have tildes. The coefficient of the trap potential becomes $(a_{\rm ho}k_0)^{-4}$ with the harmonic oscillator length $a_{\rm ho} = \sqrt{\hbar/m\omega_\perp}$. Since $a_{\rm ho}$ is a few times larger than $2\pi/k_0$ in a usual experimental situation, the coefficient of the trap potential becomes very small; we use $(a_{\rm ho}k_0)^{-4} = 0.005$ in the following calculation. The normalization of the wave function is given by the total particle number in the 2D system $N = \int d^2r \Psi^\dagger\Psi = \int d^2r(|\Psi_1|^2 + |\Psi_2|^2) = N_1 + N_2$. By replacing the wave function as $\Psi = \sqrt{N}k_0\tilde{\psi}$, where $\int d^2r|\tilde{\psi}|^2 = 1$, one can define the dimensionless 2D coupling strength as $\tilde{g}_{2d} = 2mgN/\hbar^2$ [26]. The time-dependent GP equations derived from Eq. (2) can be written as

$$i\frac{\partial\psi_1}{\partial t} = -(\nabla^2 + 2i\partial_x)\psi_1 + \frac{\delta}{2}\psi_1 + \frac{\Omega}{2}\psi_2 + V_{\rm tr}\psi_1 + g_{2d}(|\psi_1|^2 + \gamma|\psi_2|^2)\psi_1, \tag{5}$$

$$i\frac{\partial\psi_2}{\partial t} = -(\nabla^2 - 2i\partial_x)\psi_2 - \frac{\delta}{2}\psi_2 + \frac{\Omega}{2}\psi_1 + V_{\rm tr}\psi_2 + g_{2d}(|\psi_1|^2 + \gamma|\psi_2|^2)\psi_2, \tag{6}$$

where tildes are omitted in the notation. In the following, we fix $g_{2d} = 1000$ and $\delta = 0$ for simplicity. Thus, the free parameter in our study is only the Rabi frequency Ω.

B. Brief review of the ground state phases without a vortex

The starting point in our study is to understand the ground state structure without vorticity. Figure 1 summarizes the results obtained by solving Eqs. (5) and (6) via imaginary time evolution. The ground state can be distinguished by the population difference (longitudinal spin polarization) $m_z = |N_1 - N_2|/N$ with respect to Ω as, (A) the stripe phase, (B) the plane-wave (polarized) phase, and (C) the mixed (single-minimum) phase [1, 16, 17]. These phases are determined by the properties of the minima in the single-particle spectrum of the hamiltonian Eq. (1). The stripe phase is a consequence in which the condensed particles are equally populated to two degenerate minima of finite linear momenta with an opposite sign. The plane-wave phase occurs when the particles condense to either of the two degenerate minima. With increasing Ω, the two minima merge to a single minimum, which results in the mixed phase with a zero linear momentum.

The condensate wave function of this system can be written as $\psi = \sqrt{n(\mathbf{r})}\eta$ with the spinor η being approximated by the ansatz [17]

$$\eta = C_+ \begin{pmatrix} \sin\theta \\ -\cos\theta \end{pmatrix} e^{+ik_1 x} + C_- \begin{pmatrix} \cos\theta \\ -\sin\theta \end{pmatrix} e^{-ik_1 x}, \tag{7}$$

where k_1 represents the canonical momentum (in unit of k_0) where the Bose-Einstein condensation takes place and $C_\pm$ is the complex amplitude of the $\pm k_1$ component. The Rabi coupling favors the π phase difference between two components, so that the ψ_2-component has a minus sign. The angle θ can be determined by $\cos(2\theta) = k_1$, given by the energy minimization with respect to k_1 [17]. The total density $n(\mathbf{r})$ is approximately given by the Thomas-Fermi profile [27]

$$n(r) = \frac{\mu - V_{\rm tr}}{g_{2d}(1+\gamma)/2 - \Omega/(4|\psi_1||\psi_2|)}. \tag{8}$$

Although in the stripe phase the total density $n(\mathbf{r})$ is periodically modulated slightly, Eq. (8) is still good to represent the smoothed global density profile. For $\Omega \ll g_{2d}$ the usual Thoms-Fermi profile for a single-component system is reproduced as $n(r) = n(0)(1 - r^2/R_\perp^2)$, where $n(0) = 2\mu/g_{2d}(1+\gamma)$ is the condensate density at the origin ($r = 0$) and $R_\perp = \sqrt{\mu}(k_0 a_{\rm ho})^2$ is the Thomas-Fermi radius. The chemical potential is determined by the normalization condition.

The stripe phase is realized for small Ω (≤ 0.35) in our parameter setting. The wave function can be described by $|C_+| = |C_-| = 1/\sqrt{2}$ and the wave number k_1 given by

$$k_1 = \sqrt{1 - \frac{\Omega^2}{16(1+G_1)^2}}, \tag{9}$$

where $G_1 = \bar{n}g_{2d}(1+\gamma)/8$ with the mean density $\bar{n} = \int d^2r n^2(r)$. For small $\Omega \ll 1$, one can approximate $k_1 \approx$

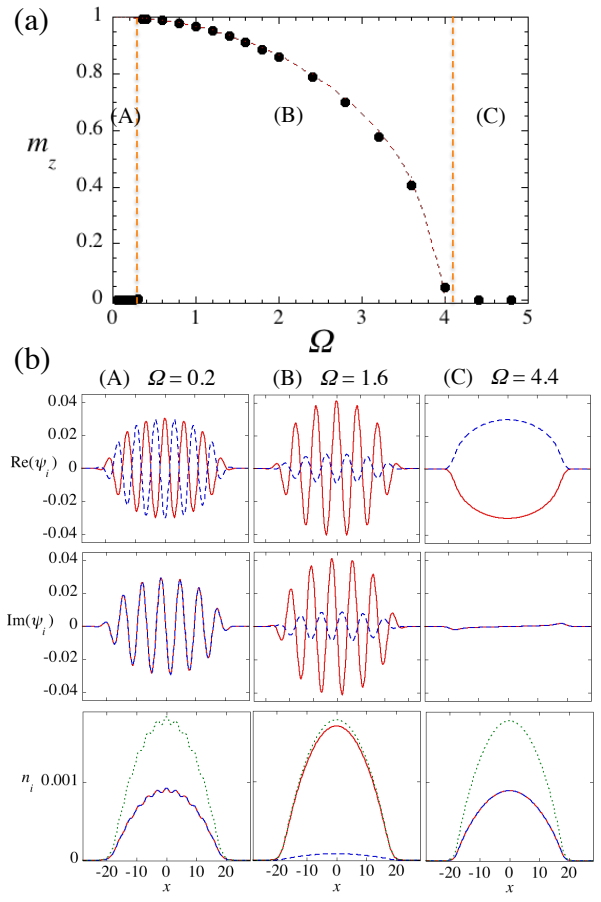

FIG. 1. (Color online) The phases of the ground states of the BEC with the laser-induced SO coupling. (a) The population difference m_z between two components as a function of Ω. The phases (A), (B), and (C) correspond to the stripe, plane-wave, and mixed phases, respectively. A dotted curve in the region (B) represents Eq. (12). The result is consistent with that of the 1D GP equation reported in Ref. [17]. (b) The cross section along $y = 0$ of the condensate wave function in each phase: the real part (upper), the imaginary part (middle), and the density in each component (bottom). The solid and dashed curves correspond to the quantities for ψ_1- and ψ_2-component, respectively. The total density is also shown in the bottom by dotted curves.

1 and thus $\theta = 0$ or π. We can eventually write the wave function as

$$\psi \simeq \frac{n(r)}{\sqrt{2}} \begin{pmatrix} e^{-ix} \\ -e^{ix} \end{pmatrix}. \tag{10}$$

Here, we take the relative phase between C_+ and C_- to be zero. Figure 1(b-A) shows that the wave function can be described by Eq. (10), where the real and imaginary parts are out-of-phase and in-phase between the two components, respectively, with respect to x.

Next, we consider the plane-wave (polarized) phase, where the condensation takes place in a single plane-wave state with either $+k_1$ or $-k_1$; we choose $+k_1$ in the discussion here. Then, $C_+ = 1$ and $C_- = 0$ and the wave function is given by

$$\psi = n(r) \begin{pmatrix} \sin\theta \\ -\cos\theta \end{pmatrix} e^{ik_1 x}, \tag{11}$$

and

$$k_1 = \sqrt{1 - \frac{\Omega^2}{16(1-2G_2)^2}} = m_z \tag{12}$$

with $G_2 = \bar{n} g_{2d}(1-\gamma)/8$. In our case, G_2 is very small parameter and actually neglected. The signature of the plane-wave phase is the finite population difference, which actually follows the relation $m_z = k_1$ as shown in Fig. 1(a). The imaginary part of the wave function becomes out-of-phase [Fig. 1(b-B)], which is also a clear difference from the stripe phase.

The third phase is the mixed (single minimum) phase, where condensation takes place at zero momentum $k_1 = 0$. Then, the wave function does not exhibit sinusoidal oscillation as seen in Fig. 1(b-C), so that the average spin polarization vanishes.

III. NUMERICAL SIMULATION OF VORTEX DYNAMICS

Here, we numerically simulate the vortex dynamics in SO coupled BECs by solving the 2D GP equations (5) and (6) [28]. We prepare a vortex at a certain position in the condensate in the following way. First, we calculate the ground state wave function without vortices by imaginary time evolution of Eqs. (5) and (6). Next, we imprint a phase defect at a certain position $\mathbf{r} = \mathbf{r}_v$ by multiplying the phase $e^{i\phi}$ with the profile $\phi(\mathbf{r} - \mathbf{r}_v) = \arctan(\frac{y-y_v}{x-x_v})$ in one or both of the components. Using this wave function as the initial state, we again proceed short imaginary time evolution, which can make the amplitude of the wave function converge to the proper profile without changing the vortex position significantly. As a result, we can prepare the initial state of real time evolution [29]. Here, we denote the winding number q_1 and q_2 of the vortex in the ψ_1- and ψ_2-component, respectively.

A. Stripe phase

First, we discuss the vortex dynamics in the stripe phase, where we choose $\Omega = 0.2$. In the simulation, we consider two situations shown in Fig. 2 as the typical initial states, where the winding number of the vortex in each component corresponds to $(q_1, q_2) = (1, 0)$ and $(1, 1)$.

From these initial states, we can find some important properties for laser-induced SO coupled BECs. Since the two-component are coupled by the uniform coherent Rabi coupling, one cannot make a vortex in one of the components without affecting the phase in the other component,

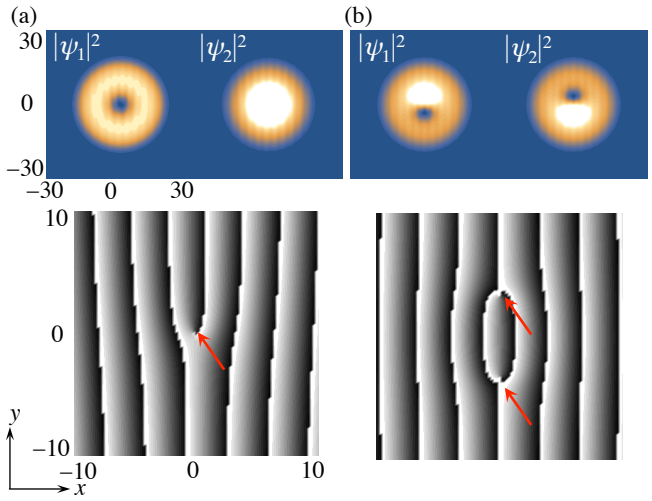

FIG. 2. (Color online) Typical initial states used in the simulations to study the vortex dynamics in the stripe phase for $\Omega = 0.2$. The vortex winding number is (a) $(q_1, q_2) = (1, 0)$ and (b) $(q_1, q_2) = (1, 1)$. The upper and lower panels represent the density profile of each component and the relative phase $\theta_1 - \theta_2$. The phase value changes from $-\pi$ (black) to π (white) continuously. The vortex is represented in the relative phase profile by arrows.

because the relative phase between the two components likes to be uniform to decrease the Rabi coupling energy. In the stripe phase, however, the Rabi coupling energy gives a minor contribution, which enable us to make vortices freely in each component. This can be seen in the phase-dependent energy of the system. When we put one vortex in each phase by multiplying the phase $\phi_i = \phi(\mathbf{r} - \mathbf{r}_{vi})$ $(i = 1, 2)$, the kinetic energy of the system is written as

$$\begin{aligned} E_k = \int d^2 r n(r) \Big\{ & |C_+|^2 \sin^2\theta \left[(v_{1x} + k_1 + 1)^2 + v_{1y}^2\right] \\ & + |C_-|^2 \cos^2\theta \left[(v_{1x} - k_1 + 1)^2 + v_{1y}^2\right] \\ & + |C_+|^2 \cos^2\theta \left[(v_{2x} + k_1 - 1)^2 + v_{2y}^2\right] \\ & + |C_-|^2 \sin^2\theta \left[(v_{2x} - k_1 - 1)^2 + v_{2y}^2\right] \Big\}, \end{aligned} \tag{13}$$

where $\mathbf{v}_i = \nabla\phi_i = (v_{ix}, v_{iy})$ is the velocity field induced by a vortex in the i-th comonent. On the other hand, the energy of the Rabi coupling is

$$E_{\rm Rabi} = -\frac{\Omega}{2} \int d^2 r n(r) \sin 2\theta \cos(\phi_1 - \phi_2). \tag{14}$$

For the stripe phase, $|C_+| = |C_-| = 1/\sqrt{2}$ and $k_1 \approx 1$, i.e., $\theta \approx 0$. Then, $E_{\rm Rabi}$ is almost zero and does not affect the system even if the relative phase is strongly disturbed. Thus, vortices can be created without costing the Rabi coupling energy. There is in principle no problem for the initial vortices to have combinations of arbitrary values of q_1 and q_2. The kinetic energy becomes $E_k \approx \frac{1}{2}(v_1^2 + v_2^2)$, which is an usual kinetic energy when vortices are put on usual two-component condensates. Therefore, vortex dynamics in the stripe phase can be approximately regarded as those in two-component BECs with a very weak coherence of the relative phase caused by a small Rabi coupling.

The above argument can be interpreted from the relative phase profile shown in the bottom of Fig. 2. The stripe phase already has a gradient $-2x$ in the relative phase because of the relatively weaker Rabi coupling than the SO coupling. Therefore, it is possible to create a single defect like $(q_1, q_2) = (1, 0)$ [Fig. 2(a)], where this vortex can be seen as a local dislocation in the relative phase profile as shown in Fig. 2(a); the $(q_1, q_2) = (1, 0)$ vortex is not allowed for other two phases, because such a single defect must break the uniform relative phase globally. On the other hands, the $(q_1, q_2) = (1, 1)$ vortex can be created with less damage of uniformity in the relative phase, as seen in Fig. 2(b). This is interpreted as the binding of two vortices by the sine-Gordon soliton of the relative phase [30] to form a vortex molecule in the coherently coupled BEC [31–33]. Although the circulations of the vortices are seen to be anti-parallel in the relative phase, this is a vortex pair with the same direction of circulations.

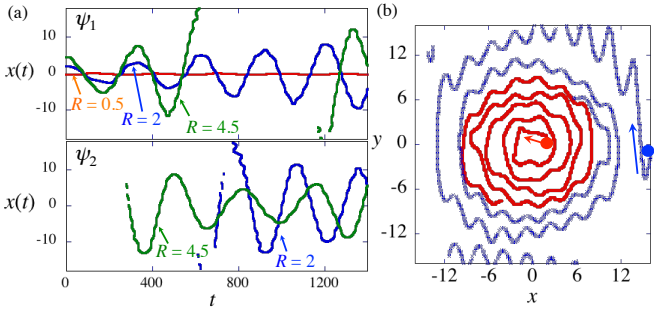

FIG. 3. (Color online) The time development of the vortex state with the winding number $(q_1, q_2) = (1, 0)$ and $\Omega = 0.2$. (a) The time development of the x-coordinate of the vortex in the ψ_1-component (upper panel) and the ψ_2-component (lower panel) for the different initial displacements $R = 0.5$, 2.0 and 4.5 from the center. (b) The vortex trajectories in the ψ_1-component (from center to outer: the red curve) and ψ_2-component (from outer to center: the blue curve) for the initial displacement $R = 2.0$.

First, we show in Fig. 3 the numerical result of vortex dynamics for the $(q_1, q_2) = (1, 0)$ vortex state, where we change the initial position $\mathbf{r}_{vi} = (R, 0)$ of the vortex. The positive displacement R from the trap center induces counterclockwise precession of a vortex around the center [5]. For a centered vortex or a slightly off-centered vortex with $R \leq 1$, the vortex is dynamically stable by keeping the small amplitude precession around the center. With increasing R, however, the amplitude of the precession becomes larger and larger over time; the vortex spirals

out as seen in Fig. 3(b). Concurrently, the vortex in the other component enters from the outer region. This conversion dynamics of the vortex is a consequence of the conservation of the total angular momentum, and actually seen in usual two-component BECs [34, 35]. For a centered vortex, a criteria of the dynamic stability is given by $g > g_{12}$, which is satisfied in our case. The stability of the off-centered vortices has not been discussed so far in two-component BECs, but our results indicate that there is some critical displacement from the center for a vortex to be dynamically unstable. The fluctuation of the trajectory seen in Fig. 3(b) is a consequence of the density modulation in the stripe phase.

Next, we turn to the $(q_1, q_2) = (1, 1)$ vortex state. In this case, each vortex is bounded by a sine-Gordon kink in the relative phase [30–33]. When the center-of-mass of the molecule is positioned at the origin, the vortex molecule undergoes self-rotation as shown in Fig. 4(a). When the center-of-mass is shifted from the origin, the trajectories of each vortex show complicated curves [Fig. 4(c)]. However, when we look at their center-of-mass coordinate $\mathbf{r}_{\rm com} = (\mathbf{r}_1 + \mathbf{r}_2)/2$ and relative coordinate $\mathbf{r}_{\rm rel} = (\mathbf{r}_1 - \mathbf{r}_2)/2$, the motion can be explained by the simple sinusoidal translation and self-rotational motion of the molecule as shown in Fig. 4(d).

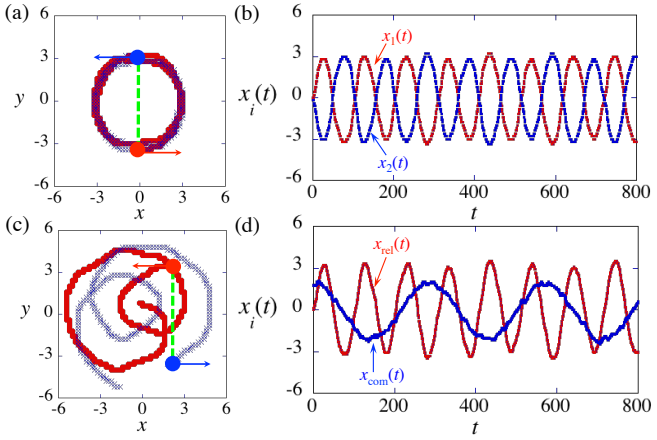

FIG. 4. (Color online) The vortex motion for $(q_1, q_2) = (1, 1)$ and $\Omega = 0.2$. The vortex molecule is initially polarized along the y-direction, in which the molecular length is 6.5 (in unit of k_0^{-1}). (a) The trajectories of each vortex. The center-of-mass of the vortex molecule are located on $(x_{\rm com}, y_{\rm com}) = (0, 0)$. The (red) circles and (blue) crosses represent the vortex positions in the ψ_1- and ψ_2-component, respectively. (b) The time development of the x-coordinates of the vortices in the ψ_1- and ψ_2-component, corresponding to (a). (c) The same as (a) but the initial position of the center-of-mass is $(x_{\rm com}, y_{\rm com}) = (2, 0)$. (d) The corresponding time development of the x-component of the center-of-mass and relative coordinates of the vortex molecule, corresponding to (c).

Figure 4 clearly shows that the vortex motion consists of two ingredients. The center-of-mass motion of the off-centered vortices can be caused by the density inhomogeneity due to the trapping potential, where the velocity of the motion is proportional to $\hat{\mathbf{z}} \times \nabla V_{\rm tr}$ [5, 23]. The analytical form of the precession frequency of a off-centered vortex is known as $\Omega = \Omega_m/(1 - r_v^2/R_\perp^2)$, where $\Omega_m = (3\hbar/2mR_\perp^2)\ln(R_\perp/\xi)$ is the critical rotation frequency that gives (meta)stability of a centered vortex and $R_\perp$ is a Thomas-Fermi radius along the radial direction. Rewriting this to the dimensionless form and using $r_v = 2$, $R_\perp \approx 20$ and $\xi \sim 1$, we get a rough estimation of the precession period $T \approx 300$ (in unit of $\hbar/E_R$), which agrees with the numerical results of $x_{\rm com}$ in Fig. 4. On the other hand, the internal rotation of the vortex molecule can be caused by a balance of the Magnus force and the intervortex force, which consists of a tension of the sine-Gordon kink and the density-density interaction between the two components [36]. The tension of the sine-Gordon kink is given by $\sigma = \bar{n}\sqrt{8\hbar^3\Omega/m}$ [30]. The intervortex force caused by the intercomponent density-density interaction is repulsive because of $g_{12} > 0$ and asymptotically has a dependence $\sim (\ln R/\xi - 1/2)/R^3$ [37]. The net force for each vortex can be written as $F_v \sim \sigma R - (\ln R/\xi - 1/2)/R^3$. The latter contribution is smaller than the former when R becomes larger, so we neglect this in the following estimation. Then, the vortex coordinate $\mathbf{r}_i$ for the i-th component is governed by the equation of motion $2\pi q_i \dot{\mathbf{r}}_i \times \hat{\mathbf{z}} = \mathbf{F}_v$ [38]. Using the formula of the tension, we get $T \approx 100$, which is fairly agreement with the numerical result.

B. Plane-wave phase

Next, we go to the discussion on the vortex dynamics in the plane-wave phase. A quite different point from the stripe phase is that the initial condition for the vortex is only limited to $(q_1, q_2) = (1, 1)$. This is because the relative phase is locked to be π over the space because of the energy constraint of $E_{\rm Rabi}$. Thus, the individual putting of the vortex on each component is prohibited. The typical initial vortex configuration of the simulation is shown in Fig. 5. We prepare a slightly off-centered vortex to promote the precession motion of the vortex. The dominant component has a well defined vortex, while the minor component has a fragile vortex which accompanies the density modulation around the core. The positions of the vortex cores are slightly displaced from each other; the vortex core is filled by the density of the other component [Fig. 5(b)]. As seen in Fig. 5(c), although the relative phase is nearly constant over the space, the vortices are bounded by the small sine-Gordon kink. Also, a small modulation of the relative phase around the vortex core can be seen in Fig. 5(c). This may be a remnant of the stripe phase, in which the kinetic-energy term with SO coupling likes to modulate the wave function. This spatial modulation may be also related with the roton-like excitation in the plane-wave phase [18]. The density modulation around the vortex core is seen in vortices in a dipolar BEC [39], which has also a roton-like minimum

in the excitation spectrum [40].

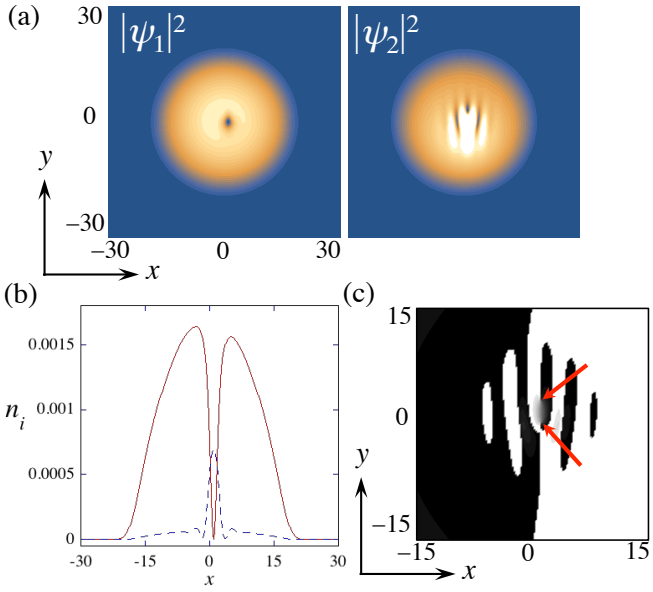

FIG. 5. Typical initial state used in the simulations in the plane-wave phase. Here we choose $(C_+, C_-) = (0, 1)$ ground state with $\Omega = 1.6$ and put the $(q_1, q_2) = (1, 1)$ vortex at $(x, y) \approx (1, 0)$ in the ψ_1-component and $(x, y) \approx (1, 3)$ in the ψ_2-component. (a) The contour plot of the condensate densities. (b) The cross section along $y = 0$, where $|\psi_1|^2$ and $|\psi_2|^2$ are plotted by solid and dashed curves, respectively. (c) The profile of the relative phase. The phase value changes from $-\pi$ (black) to π (white) continuously. The positions of the vortices are marked by arrows.

The dynamics of this vortex state is shown in Fig. 6. We can see mainly two features. First, the vortex trajectories in the two degenerate ground states are different even when the vortex motion starts from the same initial positions. The upper panel in Fig. 6 corresponds to the vortex dynamics for $(C_+, C_-) = (0, 1)$ (condensation onto $-\mathbf{k}_1$ momentum state), while the lower one does $(C_+, C_-) = (1, 0)$ (condensation onto $+\mathbf{k}_1$ momentum state). The amplitude of the precession in the upper panel looks to be smaller than that in the lower one. The asymmetry of the vortex dynamics can be understood from the kinetic energy Eq. (13). For $(C_+, C_-) = (0, 1)$, the energy can be written as

$$E_{k-} = \int d^2 r n(r) \Big\{ \cos^2\theta \left[(v_{1x} + 1 - k_1)^2 + v_{1y}^2 \right] + \sin^2\theta \left[(v_{2x} - 1 - k_1)^2 + v_{2y}^2 \right] \Big\}, \quad (15)$$

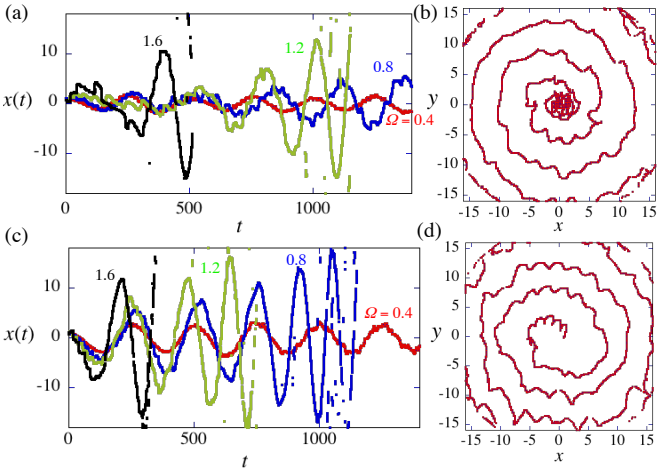

FIG. 6. The time development of the vortex position in the plane-wave phase. The initial position of the vortex in the dominant component is $(x, y) \approx (1, 0)$ The vortex trajectories in the minor component are not shown because the motion exhibits turbulent-like behavior so that it is difficult to identify the individual vortex trajectory. (a) Time development of $x_v(t)$ for $(C_+, C_-) = (0, 1)$ with $\Omega = 0.4$, 0.8, 1.2, and 1.6. (b) The vortex trajectory corresponding to (a) for $\Omega = 1.2$. (c) Time development of $x_v(t)$ for $(C_+, C_-) = (1, 0)$ with $\Omega = 0.4$, 0.8, 1.2, and 1.6. (d) The vortex trajectory corresponding to (c) for $\Omega = 1.2$.

and for $(C_+, C_-) = (1, 0)$

$$E_{k+} = \int d^2 r n(r) \Big\{ \sin^2\theta \left[(v_{1x} + 1 + k_1)^2 + v_{1y}^2 \right] + \cos^2\theta \left[(v_{2x} - 1 + k_1)^2 + v_{2y}^2 \right] \Big\}, \quad (16)$$

where the term proportional to $\cos^2\theta$ corresponds to the contribution from the dominant component. Then, we can consider that a vortex in the dominant component is dragged by a constant background velocity $\mathbf{v}_{\rm bg} = (1 - k_1)\hat{\mathbf{x}}$ for $(C_+, C_-) = (0, 1)$ and $\mathbf{v}_{\rm bg} = -(1 - k_1)\hat{\mathbf{x}}$ for $(C_+, C_-) = (1, 0)$ because of the Magnus effect. This situation is schematically shown in Fig. 7(a). For $(C_+, C_-) = (0, 1)$ $\mathbf{v}_{\rm bg}$ is opposite to the counterclockwise direction of the precession motion caused by the density gradient, so that the precession motion tends to be suppressed. On the other hand, for $(C_+, C_-) = (1, 0)$ $\mathbf{v}_{\rm bg}$ enhances the tendency of the counterclockwise precession.

Secondly, we can see the significant damping behavior of the vortex motion, which is typical for the vortex precession in the presence of dissipation [5]. The vortex spirals out to outward as seen in Fig. 6(b) and (d). Different from the motion seen in the stripe phase [Fig. 3], the vortex is not converted to the other component. However, this is questionable because dissipation is absent in our problem. One reason of this damping behavior may be due to the presence of the minor component. Because

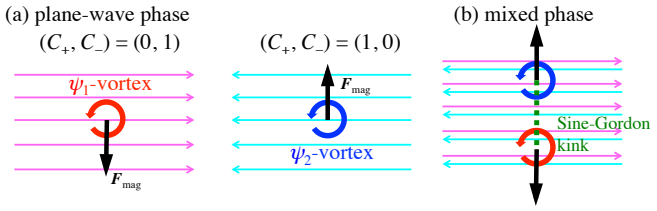

FIG. 7. Schematic illustration of the vortex propertes in (a) the plane-wave phase and (b) the mixed phase. In the plane-wave phase, we only show the dominant component. For $(C_+, C_-) = (1, 0)$, there is a background velocity along $+x$-direction, thus the Magnus force for a vortex with $q = 1$ directs to $-y$. For $(C_+, C_-) = (0, 1)$, there is a background velocity along $-x$-direction, thus the Magnus force for a vortex with $q = 1$ directs to $+y$. In the mixed phase (b), both components are equally populated and each vortex has the Magnus force with the same magnitude but the opposite direction. The vortex configuration is kept by the balance between the Magnus force and the tension of the sine-Gordon kink. Thus, the vortex molecule is polarized along the y-direction.

the amplitude of the minor component is very small, the wave function is highly excited to undergo a turbulent-like state during the time evolution, which plays the role of thermal noise for the other dominant component. Actually, the vortex decays faster and faster when the Rabi coupling is increased for the minor component to be more populated [see Fig. 6(a) and (c)]. However, as the system approaches to the mixed phase with increasing Ω further, the balance of the Magnus force and the tension of the sine-Gordon kink prohibits the vortices to go outward, effective dissipation mechanism thus being no more present in the mixed phase as shown below.

C. Mixed phase

Finally, we will discuss the vortex dynamics in the mixed phase. Since there is a strong Rabi coupling in this case, the $(q_1, q_2) = (1, 1)$ vortices are strongly bounded to form the vortex molecule. However, different from that seen in the stripe phase [Fig. 4], the vortex molecule does not show the internal rotation; its polarization is fixed to be the y-direction. In this phase, the energy is given by

$$E_{k0} = \int d^2 r n(r) \Big\{ \frac{1}{2} \left[(v_{1x} + 1)^2 + v_{1y}^2 \right] + \frac{1}{2} \left[(v_{2x} - 1)^2 + v_{2y}^2 \right] \Big\}. \quad (17)$$

Thus, the Magnus force caused the background velocity induced by the SO coupling has the same magnitude and the opposite direction. Since the vortices are attracted by the tension of the sine-Gordon kink, the exact balance between Magnus force and the kink tension stabilizes dynamically the vortex molecule at the same position. For the off-centered vortex molecule, the center-of-mass of the vortex molecule shows a circular motion around the origin without rotating the molecule itself, as shown in Fig. 8.

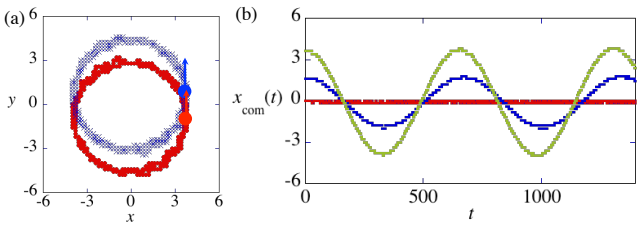

FIG. 8. The time development of the vortex position in the mixed phase with $\Omega = 4.4$. (a) The vortex trajectories of ψ_1-(red circles) and ψ_2-component (blue crosses). The initial position is indicated by large circles. (b) The time development of the x-coordinate of the center-of-mass of the two vortices, where the initial positions of the center-of-mass are changed as $x_{com} = 0$, 1.75, 3.5.

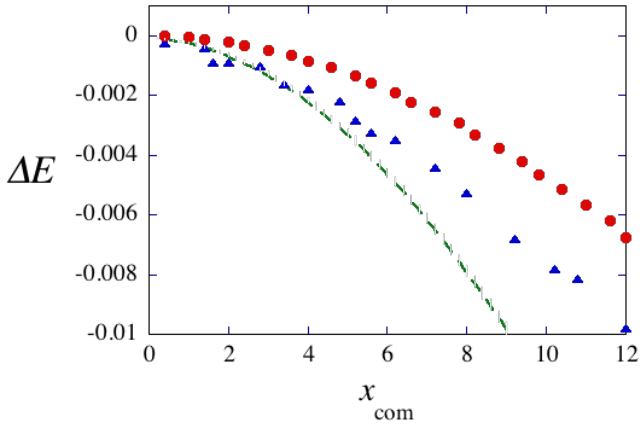

FIG. 9. The total energy as a function of the center-of-mass displacement of the vortex molecule from the center. ΔE is defined by $\Delta E = E(x_{com}) - E(0)$. The energy is calculated from the states with an off-center vortex molecule, obtained by a similar way as described in the 1st paragraph in Sec. III. The circles represent the energy of the off-centered vortex molecule in the mixed phase with $\Omega = 4.4$, while the triangles for that in the striped phase with $\Omega = 0.2$. The dashed curve shows the energy of an off-centered vortex in a single component BEC, where we consider the situation $N = N_1$ ($N_2 = 0$) without the SO coupling.

Note that the period of the center-of-mass is longer than that observed in the stripe phase in Fig. 4. The period of the vortex precession is basically determined by the gradient of the total energy with respect to the vortex position $\mathbf{r}_v$ [5, 41]. Here, we plot the energy as a function of the center-of-mass position of the vortex molecule in Fig. 9. For comparison, we also plot the same energy in the stripe phase ($\Omega = 0.2$) as well as for an off-center vortex in a single-component BEC. The energy

for the stripe phase is more or less agreed with that for a single-component BEC, especially for $x_{\rm com} < 5$. This is the reason why the precession period can be estimated by the known formula as discussed in Sec. III A. On the other hand, the slope of the energy in the mixed phase decays slower than the other cases. This indicates that the vortex molecule are stabilized against the center-of-mass displacement because of the balance of the forces shown in Fig. 7(b).

IV. DISCUSSION AND CONCLUSION

We study the vortex dynamics in laser-induced SO coupled BECs. The characteristics of the vortex dynamics is very different in each ground state phase, which can be used to identify each phase. The vortex dynamics in the stripe phase is similar to those in the conventional two-component BECs, while the plane-wave phase has asymmetric vortex dynamics in the two degenerate ground state. In the mixed phase, the polarization of the vortex molecule is kept during the dynamics, which is very different behavior seen in the conventional two-component BEC with only coherent Rabi coupling. We hope that these numerical solutions would be useful for better understanding of the vortex dynamics in exotic superfluids with SO coupling. However, we would like to point out that the understanding of the vortex dynamics in conventional two-component BECs is still incomplete, although there has been some progress recently [36, 38, 42].

ACKNOWLEDGEMENT

The author thanks Luis Santos and all members in his group for hospitality in Leibniz University Hannover. This work was partly supported by KAKENHI from JSPS (Grant No. 26400371).

[1] Y.-J. Lin, K. Jiménez-García, and I. B. Spielman, Nature(London) **471**, 83 (2011).
[2] V. Galitski and I. B. Spielman, Nature(London) **494**, 49 (2013).
[3] N. Goldman, G. Juzeliunas, P. Ohberg, I. B. Spielman Rep. Prog. Phys. **77**, 126401 (2014).
[4] H. Zhai, Rep. Prog. Phys. **78**, 026001 (2015).
[5] A. L. Fetter, Rev. Mod. Phys. **81**, 647 (2009).
[6] C. Wu and I. Mondtragon-Shem, Chin. Phys. Lett. **28**, 097102 (2011).
[7] S. Sinha, R. Nath, and L. Santos, Phys. Rev. Lett. **107**, 270401 (2011).
[8] H. Hu, B. Ramachandhran, H. Pu, and X.-J. Liu, Phys. Rev. Lett. **108**, 010402 (2012).
[9] J. Radić, T. A. Sedrakyan, I.B. Spielman, and V. Galitski, Phys. Rev. A **84**, 063604 (2011).
[10] X.-Q. Xu and J. H. Han, Phys. Rev. Lett. **107**, 200401 (2011).
[11] X.-F. Zhou, J. Zhou, and C. Wu, Phys. Rev. A **84**, 063624 (2011).
[12] J.-Y. Zhang, S.-C. Ji, Z. Chen, L. Zhang, Z.-D. Du, B. Yan, G.-S. Pan, B. Zhao, Y.-J. Deng, H. Zhai, S. Chen, and J.-W. Pan, Phys. Rev. Lett. **109**, 115301 (2012).
[13] P. Wang, Z.-Q. Yu, Z. Fu, J. Miao, L. Huang, S. Chai, H. Zhai, and J. Zhang, Phys. Rev. Lett. **109**, 095301 (2012).
[14] L. W. Cheuk, A. T. Sommer, Z. Hadzibabic, T. Yefsah, W. S. Bakr, and M. W. Zwierlein, Phys. Rev. Lett. **109**, 095302 (2012).
[15] L. Huang, Z. Meng, P. Wang, P. Peng, S.-L. Zhang, L. Chen, D. Li, Q. Zhou, J. Zhang, arXiv:1506.02861 (2015).
[16] T.-L. Ho and S. Zhang, Phys. Rev. Lett. **107**, 150403 (2011).
[17] Y. Li, L. Pitaevskii and S. Stringari, Phys. Rev. Lett. **108**, 225301 (2012).
[18] G. I. Martone, Y. Li, L. Pitaevskii and S. Stringari, Phys. Rev. A **86**, 063621 (2012).
[19] Q.-Q. Lü and D. E. Sheehy, Phys. Rev. A **88**, 043645 (2013).
[20] Y. Li, G. I. Martone, L. Pitaevskii and S. Stringari, Phys. Rev. Lett. **110**, 235302 (2013).
[21] T. Ozawa, L. P. Pitaevskii, and S. Stringari, Phys. Rev. A **87**, 063610 (2013).
[22] C. Hamner, Y. Zhang, M. A. Khamehchi, M. J. Davis, and P. Engels, Phys. Rev. Lett. **114**, 070401 (2015).
[23] A. Fetter, Phys. Rev. A **89**, 023629 (2014).
[24] C.N. Weiler, T.W. Neely, D.R. Scherer, A.S. Bradley, M.J. Davis, B.P. Anderson, Nature (London) **455**, 948 (2008).
[25] D.V. Freilich, D.M. Bianchi, A.M. Kaufman, T.K. Langin, and D.S. Hall, Science **329**, 1182 (2010).
[26] The value of N represents the particle number in the 2D plane, where the condensate is assumed to be homogeneous along the z-axis, and can be written as $N = N_{\rm 3D}/L_z$ with the typical size L_z of the z-direction.
[27] M. Abad and A. Recati, Euro. Phys. J. D **67**, 148 (2013).
[28] We would like to point out that the variational wave function introduced by Fetter [23] to study the vortex dynamics in the Lagrangian formulation is applicable only to the plane-wave phase. His trial function for the spinor is given by
$$\zeta = \begin{pmatrix} e^{i\theta_1}\cos\theta \\ -e^{i\theta_2}\sin\theta \end{pmatrix} e^{i\alpha x} \tag{18}$$
where $\theta_j = m_j \arctan\left(\frac{y-y_0}{x-x_0}\right)$ represents the vortex winding. An additional velocity contribution αx was introduced to account for the spatial asymmetry of h_0. This ansatz is nothing but the wave function of the plane-wave phase of Eq. (11), which is applicable for the range $0.3 \le \Omega \le 4$. For small $\Omega(\le 0.3)$, where the stripe phase is the ground state, the ansatz Eq. (18) cannot describe the dynamics correctly.
[29] The vortex state $(q_1, q_2) = (1, 0)$ in the stripe phase is not energetically preferable for the condensates with a intercomponent coherent coupling. During the imaginary time evolution, the interconversion of the particle number can make the non-vortex component more populated,

which reduces the total energy, and eventually eliminates the component with a vortex. Thus, we fix each particle number during the second imaginary time propagation in this case.

[30] D. T. Son and M. A. Stephanov, Phys. Rev. A **65**, 063621 (2002).

[31] K. Kasamatsu, M. Tsubota, and M. Ueda, Phys. Rev. Lett. **93**, 250406 (2004).

[32] K. Kasamatsu, M. Tsubota, and M. Ueda Phys. Rev. A **71**, 043611 (2005).

[33] M. Cipriani and M. Nitta Phys. Rev. Lett. **111**, 170401 (2013).

[34] V. M. Pérez-García and J. J. García-Ripoll, Phys. Rev. A **62**, 033601 (2000).

[35] D. V. Skryabin Phys. Rev. A **63**, 013602 (2000).

[36] L. Pitaevskii, talk at "Cold Atoms Meet High Energy Physics", 2015, Trento Italy.

[37] M. Eto, K. Kasamatsu, M. Nitta, H. Takeuchi, M. Tsubota, Phys. Rev. A **83**, 063603 (2011).

[38] K. Kasamatsu, M. Eto, and M. Nitta, in preparation.

[39] S. Yi and H. Pu, Phys. Rev. A **73**, 061602(R) (2006).

[40] T. Lahaye, C. Menotti, L. Santos, M. Lewenstein, T. Pfau, Rep. Prog. Phys. **72**, 126401 (2009).

[41] S. A. McGee and M. J. Holland Phys. Rev. A **63**, 043608 (2001).

[42] M. Eto and M. Nitta, talk at "Cold Atoms Meet High Energy Physics", 2015, Trento Italy.